



Original Article

In-line (α ,n) source sampling methodology for monte carlo radiation transport simulations

David P. Griesheimer^{*}, Andrew T. Pavlou, Jason T. Thompson, Jesse C. Holmes,
Michael L. Zerkle, Edmund Caro, Hansem Joo

Naval Nuclear Laboratory, P.O. Box 79, West Mifflin, PA 15122, USA

ARTICLE INFO

Article history:

Received 2 June 2017

Accepted 3 August 2017

Available online 1 September 2017

Keywords:

Monte Carlo

alpha particle

neutron source

continuous-slowing-down

charged particle

ABSTRACT

A new in-line method for sampling neutrons emitted in (α ,n) reactions based on alpha particle source information has been developed for continuous-energy Monte Carlo simulations. The new method uses a continuous-slowing-down model coupled with (α ,n) cross section data to precompute the expected neutron yield over the alpha particle lifetime. This eliminates the complexity and computational cost associated with explicit charged particle transport. When combined with an integrated alpha particle decay source sampling capability, the proposed method provides an efficient and accurate method for sampling (α ,n) neutrons based solely on nuclide inventories in the problem, with no additional user input required. Results from several example calculations show that the proposed method reproduces the (α ,n) neutron yields and energy spectra from reference experiments and calculations.

© 2017 Korean Nuclear Society, Published by Elsevier Korea LLC. This is an open access article under the CC BY-NC-ND license (<http://creativecommons.org/licenses/by-nc-nd/4.0/>).

1. Introduction

The ability to accurately represent the emission rate and spectrum of neutrons produced by (α ,n) reactions with light nuclides in materials containing alpha particle emitters (such as actinides) is important for critical experiment analysis, reactor design, reactor protection, and shielding applications. Examples of these applications include the modeling of artificial (Am–Be, Pu–Be, etc.) neutron sources used in critical assemblies, reactor startup, and response checks of nuclear instrumentation; neutron production in fresh and irradiated fuel in both reactors and fuel cycle facilities; and neutron shielding analyses involving spent fuel.

Support for (α ,n) sources in Monte Carlo (MC) transport codes in the past [1–5] has suffered from a variety of disadvantages. First, explicit alpha transport in codes such as MCNP, FLUKA, and GEANT is computationally expensive [1–3]. The charged particle transport code package SRIM/TRIM is generally fast but can only be used with planar geometries [4]. Additionally, there is a lack of support for elastic scattering cross sections required for explicit alpha particle transport in some Evaluated Nuclear Data File (ENDF)-format incident-alpha nuclear data libraries. In other codes, such as MCNP, users must manually specify the source distribution of alphas and/or emitted neutrons from a secondary code such as SOURCES-4C [6] owing to a lack of (α ,n) information. The MC radiation transport

code COG [5] treats explicit alpha transport with a multistep approach using the continuous-slowing-down approximation, but only the ability of the method to calculate total neutron emission rates has been studied [7].

In this paper, we describe a new methodology for in-line sampling of neutrons emitted from (α ,xn) reactions, where (α ,xn) denotes any alpha-particle reaction that emits neutrons. The proposed methodology is based on a thick-target, continuous-slowing-down model, resulting in a simpler and faster sampling algorithm relative to methods that utilize explicit charged particle transport. In addition, this paper demonstrates that many of the slowing-down parameters required for the (α ,n) source calculation can be precalculated and stored by nuclide along with other microscopic cross section data. The resulting method is straightforward to backfit into existing continuous-energy MC codes.

When coupled with an in-line decay source capability and suitable (α ,xn) cross sections, the new methodology produces effective neutron source distributions based only on nuclide inventories in the model. This enables calculations such as subcritical multiplication of highly depleted fuel, improves quality assurance for complex models, and simplifies user input.

2. In-line (α ,n) source generation

The production rate of neutrons due to (α ,xn) reactions is given by the basic relationship,

^{*} Corresponding author.

E-mail address: david.griesheimer@unnpp.gov (D.P. Griesheimer).

$$S_n(E_n) = \int_0^\infty y(E_\alpha) p(E_n|E_\alpha) S_\alpha(E_\alpha) dE_\alpha, \quad (1)$$

where $S_n(E_n)$ and $S_\alpha(E_\alpha)$ are the emission rates of neutrons and alpha particles, respectively, as a function of energy for the corresponding particle type, $y(E_\alpha)$ is the total yield of neutrons from (α, xn) reactions resulting from an alpha particle with initial energy E_α , and $p(E_n|E_\alpha)$ is the probability that the (α, xn) reaction induced by an alpha particle with energy E_α will produce a neutron with energy E_n .

In order to determine the neutron production rate during an MC transport simulation, it is necessary to develop on-the-fly methods for determining the neutron yield and sampling from the energy distribution of emitted neutrons from (α, xn) reactions.

2.1. Determination of neutron yield

The expected number of neutrons created by an alpha particle with initial energy E_α traveling through material m is given by

$$y_m(E_\alpha) = \sum_{i=1}^{I_m} \sum_{j=1}^{J_i} N_i \int_{E_{0,ij}}^{E_\alpha} \left(\frac{v_{ij}(E') \sigma_{ij}(E')}{-(dE'/dx)_m} \right) dE', \quad (2)$$

where I_m is the number of unique nuclides in material m , J_i is the number of (α, xn) reaction types for nuclide i , N_i is the atomic number density of nuclide i (in atoms/(barn·cm)), σ_{ij} is the microscopic neutron production cross section for (α, xn) reaction j of nuclide i , v_{ij} is the number of neutrons emitted in reaction j of nuclide i , $E_{0,ij}$ is the threshold energy for reaction j of nuclide i , and $-(dE'/dx)_m$ is the stopping power (in eV/cm) for alpha particles in material m .

For alpha particles with energy less than 20 MeV traveling in materials with atomic number greater than 20, the stopping power in eV/cm can be well approximated by the Alsmiller–Estabrook correlation [8],

$$-(dE'/dx)_m \approx \sum_{i=1}^{I_m} N_i \epsilon_i(E') \quad [\text{eV/cm}], \quad (3)$$

where $\epsilon_i(E')$ is the empirically measured function

$$\epsilon_i(E') = 1.866 \times 10^{13} \sqrt{\frac{Z_i}{E'}} \quad [\text{eV} \cdot \text{barn}] \quad (4)$$

for E' in eV. Substituting Eqs. (3) and (4) into Eq. (2) and factoring out constant terms yields

$$y_m(E_\alpha) = \omega_m \sum_{i=1}^{I_m} \sum_{j=1}^{J_i} N_i \left(\int_{E_{0,ij}}^{E_\alpha} v_{ij}(E') \sigma_{ij} E' \sqrt{E'} dE' \right), \quad (5)$$

where ω_m is the slowing-down parameter for material m ,

$$\omega_m \equiv \frac{1}{(1.866 \times 10^{13}) \sum_{i=1}^{I_m} N_i \sqrt{Z_i}}. \quad (6)$$

Note that the integral in Eq. (5) is an intrinsic (microscopic) quantity that is proportional to the number of neutrons produced by (α, xn) reaction j of nuclide i as an alpha particle with initial energy E_α slows down to the energy threshold for the corresponding reaction. In the remainder of this paper, this quantity will be referred to as the microscopic integral neutron production for reaction j in nuclide i , and is denoted by

$$\tau_{ij}(E) \equiv \int_{E_{0,ij}}^E v_{ij}(E') \sigma_{ij}(E') \sqrt{E'} dE'. \quad (7)$$

Because Eq. (7) does not depend on the density of other nuclides in the material, τ_{ij} can be precomputed and stored along with other microscopic cross section data for each nuclide.

Substituting the definition for τ_{ij} into Eq. (5) yields

$$y_m(E_\alpha) = \sum_{i=1}^{I_m} \sum_{j=1}^{J_i} \omega_m N_i \tau_{ij}(E_\alpha). \quad (8)$$

Note that the right-hand side of Eq. (8) is similar to the definition for a macroscopic cross section, with τ_{ij} acting as a microscopic cross section and $\omega_m N_i$ acting as an effective number density. The latter term accounts for both the actual number density of nuclide i , as well as the effects of the material composition on the alpha-slown-down process. Because the factor ω_m is based only on the density of nuclides in the local material, it can be calculated on the fly when time-in-life-dependent number densities are retrieved for calculating macroscopic cross sections at each alpha particle source site. As a result, calculation of the (α, xn) neutron yield using Eq. (8) is especially easy to back fit into a continuous-energy MC particle transport code using the existing framework for calculating macroscopic cross sections.

Given the similarity of $y_m(E_\alpha)$ to a macroscopic cross section, it is straightforward to define the partial neutron yields by reaction, $y_{m,ij}(E_\alpha)$, and by nuclide, $y_{m,i}(E_\alpha)$, as

$$y_{m,ij}(E_\alpha) \equiv \omega_m N_i \tau_{ij}(E_\alpha), \quad (9)$$

and

$$y_{m,i}(E_\alpha) \equiv \sum_{j=1}^{J_i} y_{m,ij}(E_\alpha) = \sum_{j=1}^{J_i} \omega_m N_i \tau_{ij}(E_\alpha), \quad (10)$$

respectively. These partial yield values will be used in the sampling algorithm described in the following sections.

Before continuing, it is useful to consider some details regarding the alpha-slown-down approximation used in the preceding derivation. Note that the proposed formulation of neutron yield as a pseudo-macroscopic cross section [Eq. (10)] is based on the Alsmiller–Estabrook correlation, which relates alpha stopping power to the sum of slowing-down contributions from each constituent nuclide in the material [Eq. (3)]. As a result, the factorization of the (α, n) yield expression into the macroscopic cross section form shown in Eq. (5) is especially straightforward. Although other approximations for alpha stopping power are available, few (if any) of these approximations allow such a convenient factorization of the (α, n) neutron yield. For example, the Bethe–Bloch expression for stopping power is a function of $\ln(E)/E$ plus additional terms (e.g., excitation potential, shell corrections) that depend on $1/E$ [9]. As a consequence, the resulting factorization, where possible, would require multiple pre-computed energy integral factors rather than just one when using the Alsmiller–Estabrook correlation.

In addition to the convenient factorization, internal testing suggests that the Alsmiller–Estabrook correlation provides an accurate estimate of alpha stopping power to lower energies than the Bethe–Bloch expression. In a 1973 study, Nitzki and Matzke [10] measured stopping power for alpha particles in UO_2 , PuO_2 , and ThO_2 , and showed that the Bethe–Bloch approximation compares well with experimental measurements down to about 4 MeV.

However, informal studies involving UO₂ indicate that the stopping powers calculated with the Alsmiller–Estabrook correlation compare well with the 1973 experimental results from Nitzki and Matzke down to 2 MeV. The 2–4 MeV energy range is especially important for in-line (α, n) calculations because many important decay alphas are emitted with energies between 4 and 6 MeV. This further supports the use of the Alsmiller–Estabrook correlation for these types of calculations. However, a thorough comparison between available alpha slowing-down approximations is beyond the scope of this paper.

2.2. Correction for α escape

The preceding derivations are based on the thick-target approximation and implicitly assume that the alpha particle will not leave the material that it was born in. In cases where the thick-target approximation is not reasonable, the source sampling methodology can be modified to account for the probability the alpha particle will escape from the material that it was originally born in. Furthermore, in volumes that contain a heterogeneous mixture of materials, it is possible for an alpha particle to travel through multiple materials before losing all of its energy [11]. For example, this situation occurs in Am–Be neutron source capsules that are manufactured by mixing AmO₂ and Be powders.

Consider an alpha particle with energy $E_{\alpha, m}$ that enters (or is born in) material m . Furthermore, let Δx_m denote the distance that the alpha particle will travel before reaching the boundary of material m . Note that Δx_m may be computed based on the current position and direction of the alpha particle (if the material heterogeneity is explicitly represented) or randomly sampled from a nearest-neighbor distribution (NND) (if the material heterogeneity is modeled stochastically). Applying the basic relationship between range and stopping power for a charged particle gives

$$\Delta x_m = \int_{E_{\alpha, m+1}}^{E_{\alpha, m}} \left(\frac{1}{-(dE'/dx)_m} \right) dE', \quad (11)$$

where $E_{\alpha, m+1}$ denotes the energy of the alpha particle when it exits material m and enters material $m + 1$.

Applying the Alsmiller–Estabrook correlation for stopping power [Eq. (3)] to Eq. (11) yields

$$\Delta x_m = \omega_m \int_{E_{\alpha, m+1}}^{E_{\alpha, m}} \sqrt{E'} dE' = \frac{2\omega_m}{3} (E_{\alpha, m}^{3/2} - E_{\alpha, m+1}^{3/2}), \quad (12)$$

which gives a relationship between Δx_m , $E_{\alpha, m}$, and $E_{\alpha, m+1}$. Note that Eq. (12) is only satisfied when

$$\Delta x_m \leq \frac{2\omega_m}{3} E_{\alpha, m}^{3/2}, \quad (13)$$

indicating that the alpha particle will reach the material boundary before losing all of its energy. If the condition in Eq. (13) is satisfied, the energy of the alpha particle when it leaves material m can be determined by solving Eq. (12) for $E_{\alpha, m+1}$

$$E_{\alpha, m+1} = \left(E_{\alpha, m}^{3/2} - \frac{3\Delta x_m}{2\omega_m} \right)^{2/3}. \quad (14)$$

The neutron yield within material m can then be determined by using $E_{\alpha, m+1}$ as the lower limit of integration in Eqs. (2) and (5)

$$y_m(E_\alpha) = \omega_m \sum_{i=1}^{I_m} \sum_{j=1}^{J_i} N_i \left(\int_{E_{\alpha, m+1}}^{E_{\alpha, m}} v_{ij}(E') \sigma_{ij}(E') \sqrt{E'} dE' \right). \quad (15)$$

Furthermore, Eq. (15) can be written in terms of the microscopic integral neutron production τ_{ij} as

$$y_m(E_\alpha) = \sum_{i=1}^{I_m} \sum_{j=1}^{J_i} \omega_m N_i (\tau_{ij}(E_{\alpha, m}) - \tau_{ij}(E_{\alpha, m+1})). \quad (16)$$

Note that Eq. (16) reverts to the original form [Eq. (10)] when the exiting alpha energy $E_{\alpha, m+1}$ is less than or equal to the minimum (α, n) reaction threshold energy for the material.

In cases where the alpha particle can travel through multiple materials during slowing down, the neutron yield in each segment can be determined using the process outlined above. The alpha transport calculation iterates over each material sequentially, using the exiting alpha energy from one material as the entering alpha energy for the next material. In these situations, it is important to note that the alpha particle cannot be safely terminated until it falls below the lowest (α, n) threshold energy for any nuclide/reaction present in the collection of materials that the alpha particle may pass through. An example that illustrates the effects of alpha transport in a heterogeneous material on (α, n) production is provided in Section 3.

2.3. (α, n) Source sampling algorithm

The process for sampling secondary neutrons produced via (α, xn) reaction(s) for a given incident alpha particle consists of three basic steps. First, the expected yield of neutrons from each nuclide and reaction type is determined and the number of secondary neutrons is sampled in proportion to the corresponding yield(s). Next, for each secondary neutron produced, the energy of the alpha particle immediately prior to the corresponding (α, xn) reaction is sampled. Finally, the initial energy and direction of each secondary neutron produced in the reaction is sampled based on the target nuclide, reaction type, and energy of the incident alpha particle at the time of the (α, xn) reaction. Note that the initial position of the neutron is assumed to be the same as the birth location of the parent alpha particle.

For the first step, there are several unbiased algorithms for sampling the neutron production by nuclide and reaction. The most straightforward approach is to independently sample the number of neutrons produced for each (α, xn) reaction of each nuclide. This sampling strategy produces a separate realization for the number of neutrons from each nuclide and reaction combination. However, the disadvantage of this approach is that it requires a sampling step for all possible (α, xn) reactions within the material. For cases where alpha-induced neutron production is dominated by a few nuclides and/or reaction types, this methodology can be inefficient because it is performing sampling on many reactions that have a low probability of producing secondary neutrons.

An alternative sampling strategy is to first sample the total number of secondary neutrons and then determine which nuclide and reaction produced each neutron based on the corresponding marginal probability distributions. In this case, the total number of secondary neutrons produced from (α, xn) reactions is given by

$$\tilde{n}_m \equiv \lfloor y_m(E_\alpha) \rfloor + \tilde{b}, \quad (17)$$

where $y_m(E_\alpha)$ is the total neutron yield for an alpha particle with energy E_α slowing down in material m and \tilde{b} is a realization from the Bernoulli random variable B , with probability of success given by

$$p = y_m(E_\alpha) - [y_m(E_\alpha)] \quad (18)$$

The probability that a secondary neutron was produced because of an (α, xn) reaction with nuclide i is given by the discrete probability density function (PDF)

$$p_i(E_\alpha) = \frac{y_{m,i}(E_\alpha)}{y_m(E_\alpha)} \quad (19)$$

Similarly, the probability that a secondary neutron from an (α, xn) reaction with nuclide i was created by reaction j is given by the conditional discrete PDF

$$p_{ji}(E_\alpha) = \frac{y_{m,ij}(E_\alpha)}{y_{m,i}(E_\alpha)} \quad (20)$$

Based on Eqs. (19) and (20), selection of the target nuclide i and (α, xn) reaction type j is possible using any unbiased discrete sampling algorithm.

Once the target nuclide and reaction type have been sampled, the energy of the alpha particle at the time of the (α, xn) reaction must be determined, which requires information on the relative probability that a partially slowed alpha particle with any energy $E'_\alpha < E_\alpha$ will produce a neutron via the (α, xn) reaction. Information on this slowing-down reaction probability distribution can be inferred from the ratio of the expected neutron production for an alpha particle at energy E'_α to the expected total neutron production from the original energy of the alpha particle, E_α ,

$$P_{m,ij}(E'_\alpha) = \frac{y_{m,ij}(E'_\alpha)}{y_{m,ij}(E_\alpha)} = \frac{\tau_{ij}(E'_\alpha)}{\tau_{ij}(E_\alpha)} \quad (21)$$

which gives the cumulative distribution function (CDF) of the desired distribution as a function of the slowing-down energy E'_α , expressed in terms of the microscopic integral production for reaction j in nuclide i , τ_{ij} .

The energy of the alpha particle immediately prior to (α, xn) reaction j with target nuclide i can be sampled from the slowing-down reaction probability distribution using the CDF given in Eq. (21). The most basic sampling algorithm is to simply draw a uniformly distributed random number ξ between 0 and 1 and then find the corresponding alpha particle energy E'_α such that $P(E'_\alpha) = \xi$. However, this sampling methodology implicitly assumes that the underlying probability distribution is a histogram. If necessary, accuracy of the energy sampling method can be further improved by sampling within the selected CDF bin according to the slope of the corresponding microscopic (α, xn) cross section values within the bin. The assumption of a linear CDF within each energy bin is reasonable, provided that the spacing between tabulated cross section values is sufficiently small. Additional accuracy can be obtained by calculating and storing the underlying PDF $p_{m,ij}(E'_\alpha)$ based on the raw cross section data, at the cost of additional data processing and cross section data storage.

2.4. Secondary neutron distributions

Once the target nuclide, reaction type, and alpha particle reaction energy have been sampled, the energy and direction of the emitted neutron can be sampled from the corresponding secondary energy distribution provided in the evaluated nuclear data. The JENDL/AN-2005 library includes (α, xn) reaction data for 17 isotopes with significance in nuclear fuel cycle applications [12]. Within these evaluations, cross section data are provided for a total of 139 distinct reactions, along with secondary neutron distributions for 36 of these reactions. The difference between the number of reactions and secondary distributions is due to the fact that only the

evaluations for ^9Be and ^{12}C provide secondary energy distributions for (α, n) reactions by discrete excitation level. The remaining nuclides combine the secondary neutron energy distributions from all (α, xn) reactions (ground state plus excited states) into a single distribution.

Secondary energy distribution data in JENDL/AN-2005 is given as a coupled energy-angle distribution (ENDF File 6) using either Kalbach–Mann systematics [13,14] or a two-body kinematics representation (used for level excitation reactions for ^9Be and ^{12}C only). Methodologies for interpreting and sampling from distributions in either of these formats are published in the documentation for the ENDF format [15].

Kalbach–Mann systematics were originally developed to model reactions for various incident charged particles with energies significantly higher (several hundred MeV) than those of interest for this work. For nuclides examined in this work, the (α, n) neutron energy and angle distributions predicted by the JENDL/AN-2005 library evaluations using Kalbach–Mann systematics compared poorly to measured neutron spectra for experiments involving lower-energy alphas characteristic of transuranic nuclide decay, as demonstrated in Section 3. In particular, the predicted neutron energy spectra based on Kalbach–Mann systematics were consistently biased too low in energy.

For many engineering applications, accurately representing the neutron energy distribution is much more important than the angular distribution. Neutron energies can impact detector sensitivity, subcritical multiplication, shielding penetration, and other physical effects. By considering the incident alpha energy, reaction Q value, compound nucleus excitation levels, and partial cross sections for ground state and level excitation reactions, the neutron energy distribution can be calculated using two-body kinematics given an assumed center-of-mass angular distribution. The energy-angle distributions predicted by JENDL/AN-2005 evaluations that use Kalbach–Mann systematics are inconsistent with two-body kinematics based on the provided data for level excitation energies and partial cross sections.

For nuclides examined in this work, neutron energy distributions predicted using two-body kinematics assuming isotropic center-of-mass neutron emission compare reasonably well with experimentally measured data, as demonstrated in Section 3. Physically, angular distributions are known to be somewhat forward peaked. The use of a forward-peaked angular distribution will tend to redistribute the energy spectrum toward higher energies, which may be important for certain applications such as shielding analyses, which can be sensitive to neutron energy.

3. Numerical results

A version of the proposed in-line (α, n) source sampling capability was implemented in a developmental version of MC21 [16], an in-house continuous-energy MC radiation transport code. Processing of the raw ENDF-format (α, n) cross section data and calculation of the microscopic integral neutron production values [Eq. (7)] was performed by NDEX [16], an in-house code for creating continuous-energy cross sections for MC21. In all cases, JENDL/AN-2005 cross-section evaluations were used for (α, n) reactions, with modifications to the neutron energy-angle distributions as specified.

In order to demonstrate the effectiveness of the new (α, n) source sampling method, a series of three example problems were considered and MC21 results compared with experimental measurements, where available, or independent calculations using the SOURCES-4C computer code. SOURCES-4C [6] is the current *de facto* standard for calculating the neutron yield and energy spectrum from the (α, n) and spontaneous fission (SF) reactions in neutron source materials. SOURCES-4C can calculate neutron production

rates and spectra for four geometric configurations (homogenous, beam, two-region interface, and three-region interface). The (α ,n) spectra in SOURCES-4C are determined assuming an isotropic neutron angular distribution in the center-of-mass frame with a library of 89 nuclide decay alpha spectra and 24 sets of product-nuclide discrete-level branching fractions. The (α ,n) reaction cross sections are drawn from a variety of sources, including an evaluation by Geiger and van der Zwan [17] for ^9Be and Perry and Wilson [18] for $^{17,18}\text{O}$.

3.1. (α ,n) Source in UO_2

In the first example, the in-line source methodology in MC21 was used to calculate the total neutron production due to (α ,n) reactions with ^{17}O and ^{18}O in a thick target of UO_2 . This example models the UO_2 thick-target measurements by Bair and Gomez del Campo [19] and West and Sherwood [20], which are two of the primary measurements used to develop the ^{17}O and ^{18}O evaluations in JENDL/AN-2005 [12]. In addition, the JENDL/AN-2005 evaluation report for (α ,xn) reaction data provides calculated and experimental neutron yield results for $^{18}\text{O}(\alpha$,n) reactions in UO_2 [12], which serves as a useful benchmark for validating the in-line (α ,n) source sampling method as implemented in MC21.

For the initial test of the in-line (α ,n) source capability, ^{17}O and ^{18}O (α ,n) neutron production in UO_2 was calculated as a function of incident alpha particle energy. In this test, a total of 14 simulations were run, with incident monoenergetic alpha particle energies ranging from 2 MeV to 15 MeV in 1-MeV increments, which covers the range of yield results provided by Boles et al. [11]. The target material for the MC21 simulation was modeled as an infinite medium of UO_2 with 2.4% enriched uranium and natural isotopic abundances of oxygen, as shown in Table 1.

Each simulation included a fixed source calculation with 10,000 total alpha source particles divided among 100 batches. The target birth weight of secondary neutrons was set to a value between 1×10^{-7} and 1×10^{-10} in order to boost the yield of neutrons produced in (α ,xn) reactions [21] so that the total number of sampled neutrons was between 1 and 100 per source alpha particle (1×10^4 to 1×10^6 secondary neutrons produced per simulation). After each simulation, the (α ,xn) neutron yield was estimated from the total birth weight of secondary neutrons produced during the simulation divided by the total number of initial alpha source particles. JENDL/AN-2005 alpha cross section data was used for all simulations.

The resulting neutron yield curve as a function of incident alpha particle energy from the 14 independent MC21 simulations is shown in Fig. 1. The results from this curve show excellent agreement with experimental works by Bair and Gomez del Campo [19] and West and Sherwood [20]. These results suggest that the proposed in-line (α ,n) sampling method is working as intended and is capable of faithfully reproducing (α ,xn) reaction rates as specified by the provided nuclear data evaluation.

In order to test the coupling between the in-line alpha decay and (α ,n) source capabilities, MC21 was used to calculate the naturally

occurring neutron source intensity and spectrum due to (α ,n) reactions caused by alpha particles emitted during the radioactive decay of uranium isotopes in the thick-target UO_2 sample. The MC21 simulation for this case used 1×10^6 source alpha particles sampled from the alpha decay spectra of ^{234}U , ^{235}U , and ^{238}U , using the in-line decay source sampling capability in MC21 [22]. The birth weight of neutrons was set to 1×10^{-6} , which increases the number of sampled secondary (α ,n) neutrons by a factor of one million, as described by Griesheimer and Nease [21]. The calculation used the JENDL/AN-2005 library for alpha cross section data and the JEFF 3.1.1 library for decay data.

Results from the simulation indicate a naturally occurring (α ,n) neutron source rate density of 6.248×10^{-4} neutrons/(s·g UO_2), based on an alpha source rate density of 5.131×10^4 alphas/(s·g UO_2). As expected, the calculated (α ,n) neutron source is small compared with the SF source rate density of 1.168×10^{-2} neutrons/(s·g UO_2) for UO_2 . SF neutrons were included in the MC21 simulation to enable comparisons with SOURCES-4C (which reports SF neutron sources). The MC21 neutron source rates agree to within 2% of the corresponding values produced by an independent simulation with the SOURCES-4C code (6.248×10^{-4} (α ,n) neutrons/(s·g UO_2) and 1.172×10^{-2} SF neutrons/(s·g UO_2)). Fig. 2 shows the sampled alpha emission spectrum and corresponding alpha reaction rate density for the simulation, confirming that MC21 is modeling the slowing down behavior of the alpha particles. Note that the resulting alpha absorption spectrum follows the characteristic shape of the $^{18}\text{O}(\alpha$,xn), which is overlaid in Fig. 2 for comparison. Note that the cross sections for ^{17}O are negligibly small compared to ^{18}O and are not included in Fig. 2.

Fig. 3 shows the naturally occurring (α ,n) neutron emission spectrum in UO_2 computed with both MC21 and SOURCES-4C. Note that the MC21 calculation using the original JENDL/AN-2005 evaluations for ^{17}O and ^{18}O (utilizing Kalbach–Mann systematics) produces a neutron emission spectrum that is strikingly different from the corresponding spectrum calculated with SOURCES-4C. In particular, this MC21 emission spectrum is significantly shifted toward lower energies, with the most probable neutron energy occurring at 750 keV vice 2.25 MeV in the SOURCES-4C spectrum. This difference is likely due to the use of the Kalbach–Mann representation of the secondary neutron energy and angular distribution for ^{17}O and ^{18}O in JENDL/AN-2005.

In order to test the hypothesis that the Kalbach–Mann representation was responsible for the shift in the neutron energy spectrum, the JENDL/AN-2005 evaluations for ^{17}O and ^{18}O were manually modified to use two-body kinematics with isotropic neutron emission in the center-of-mass frame. In the modified evaluations, each excited level of the recoil nucleus was represented explicitly, based on the partial reaction cross sections and corresponding Q values provided in the ENDF File 3 for each (α ,n) reaction.

The MC21 (α ,n) neutron emission spectrum using the modified reaction data for ^{17}O and ^{18}O (with explicit two-body kinematics) is also shown in Fig. 3. Note that the resulting spectrum shows significantly better agreement with respect to the spectrum calculated by SOURCES-4C. The absolute neutron source density also matches SOURCES-4C to within a few percent. Experimental data by Jacobs and Liskien [23] is also overlaid for comparison. This experiment used natural UO_2 and an artificial high-intensity 4.5 MeV alpha source. The alpha source intensity was sufficient to allow SF neutrons to be neglected. The MC21 spectrum using the modified JENDL/AN-2005 evaluations appear to be very consistent with the experimental spectra.

The emission spectrum from the MC21 calculation using secondary neutron energy and angle distributions based on two-body kinematics clearly shows the contributions of reactions that leave

Table 1
 UO_2 composition definition.

Nuclide	Nuclide density [nuclides/(b·cm)]	Isotopic abundance (at.%)
^{16}O	4.5829×10^{-2}	99.753
^{17}O	1.7457×10^{-5}	0.038
^{18}O	9.6000×10^{-5}	0.209
^{234}U	4.4843×10^{-6}	0.020
^{235}U	5.5815×10^{-4}	2.430
^{238}U	2.2408×10^{-2}	97.551

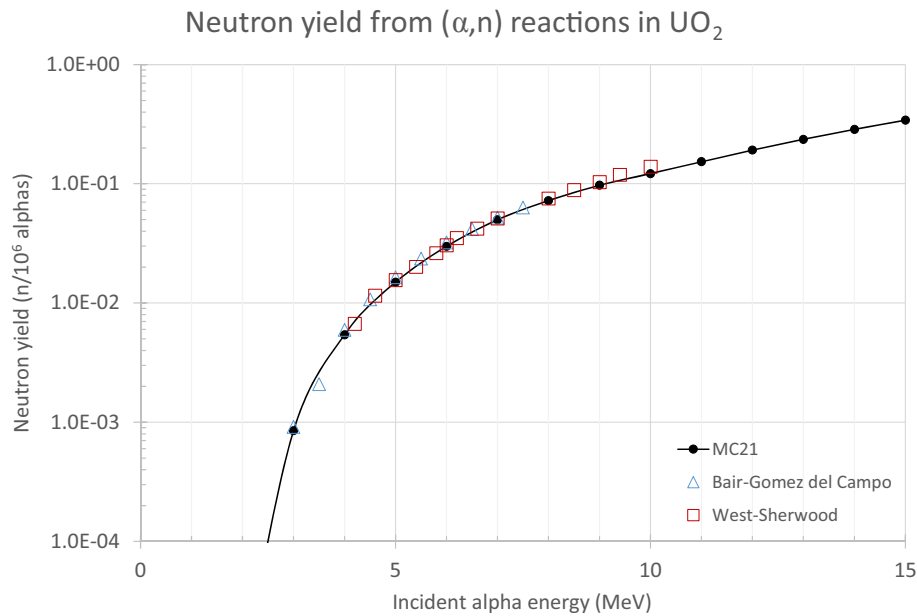


Fig. 1. Yield of neutrons from (α,n) reactions with ^{17}O and ^{18}O as a function of incident alpha particle energy computed with in-line (α,n) source sampling methodology implemented in MC21 (black) and compared to experimental results (blue [19] and red [20]).

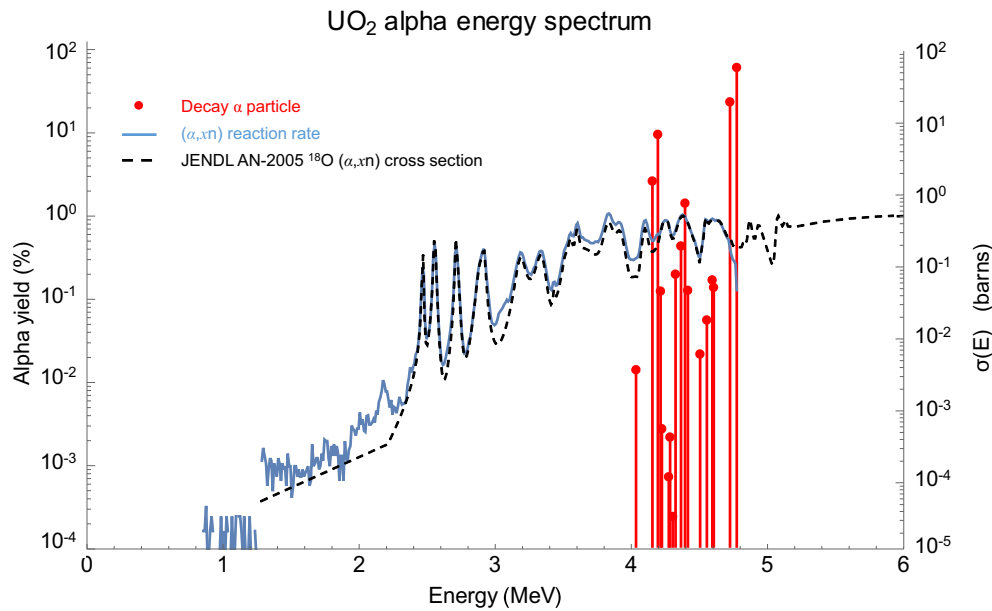


Fig. 2. Spectrum of alpha decay energies and (α,n) absorption rate for 2.4% enriched UO_2 . Also shown is the microscopic total (α,xn) cross section for ^{18}O , illustrating the relationship between the (α,n) reaction rate and cross section. Cross sections for ^{17}O are not shown because they are negligibly small compared to ^{18}O .

the recoil ^{21}Ne nucleus in the ground state (peak centered at ~ 2.25 MeV) vice reactions that leave ^{21}Ne in an excited state (peak centered at ~ 500 keV), consistent with results from experimental measurements by Jacobs and Liskien [23]. The primary differences between the emission spectra calculated using SOURCES-4C and the two-body kinematics representation in MC21 are likely attributable to underlying differences in the nuclear data used by the different codes; in particular, the branching fractions for each of the excited levels for the recoil nucleus. Note that these differences, as well as the larger differences between the Kalbach–Mann and two-body kinematics representations, only affect the energy and angular distribution of secondary neutrons emitted

during (α,n) reactions. These differences do not have any impact on the total emission rate of (α,n) neutrons, which agrees to within 2% for all methods considered.

3.2. Naturally occurring neutron source in PuO_2

In the second example, MC21 was used to determine the total naturally occurring neutron source for PuO_2 , including contributions from both (α,n) reactions as well as SF. The cross section libraries, problem setup, and running strategy are identical to the previous UO_2 example, with 1×10^6 decay alphas produced within an infinite medium of PuO_2 . The composition, shown in Table 2, is

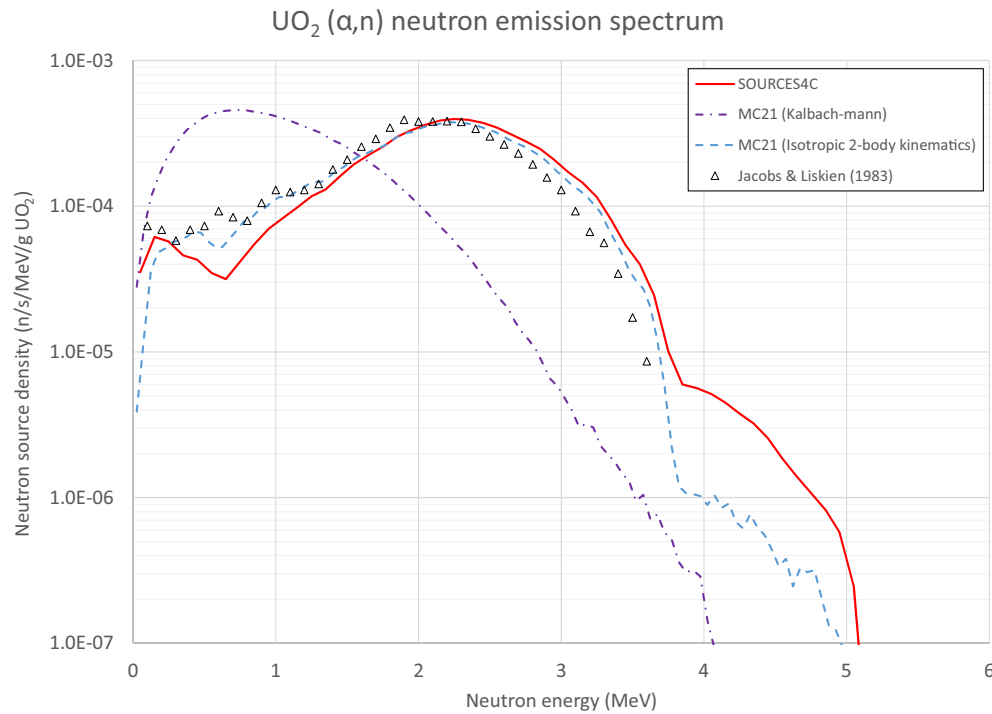


Fig. 3. Comparison of naturally occurring neutron emission spectrum due to (α, n) reactions in 2.4% enriched UO_2 , as calculated by SOURCES-4C, MC21 using the original JENDL/AN-2005 evaluations for ^{17}O and ^{18}O (with Kalbach–Mann systematics), and MC21 using modified evaluations for ^{17}O and ^{18}O using two-body kinematics for the secondary neutron energy and angular distributions. The Jacobs and Liskien [23] experimental data are for natural UO_2 using a high-intensity artificial 4.5 MeV alpha source.

Table 2
 PuO_2 composition definition.

Nuclide	Nuclide density [nuclides/(b·cm)]	Isotopic abundance (%)
^{16}O	1.1877×10^{-2}	99.757
^{17}O	4.5241×10^{-6}	0.038
^{18}O	2.4406×10^{-5}	0.205
^{238}Pu	4.8385×10^{-3}	81.280
^{239}Pu	8.9006×10^{-4}	14.952
^{240}Pu	1.7136×10^{-4}	2.879
^{241}Pu	4.7075×10^{-5}	0.791
^{242}Pu	5.8600×10^{-6}	0.098

based on a $^{238}\text{PuO}_2$ sample used for (α, n) measurements in 1968 by Herold [24] to determine shielding requirements for the $^{238}\text{PuO}_2$ heat sources used in isotopic power generators. Again, the in-line decay source capability of MC21 was used to sample alpha particles as well as SF neutrons produced from the radioactive decay of ^{238}Pu – ^{242}Pu . In this case, the neutron birth weight was set to 1×10^{-8} (for (α, n) reactions only), which increases the number of sampled secondary (α, n) neutrons by a factor of 100 million.

For this configuration and composition, MC21 estimates a total neutron production rate density of 1.203×10^4 neutrons/(s·g PuO_2), with 84.27% from (α, n) reactions and the remainder from SF. In this case, these values agree to within 0.2% when compared to results from an independent SOURCES-4C calculation (1.205×10^4 neutrons/(s·g PuO_2) with 84.32% from (α, n) reactions). Fig. 4 shows the sampled alpha emission spectrum and corresponding (α, n) reaction rate density for the simulation. Again, the (α, n) reaction rate shows a strong correlation with the ^{18}O (α, n) cross section, as expected.

Fig. 5 shows the total naturally occurring neutron emission spectrum in PuO_2 computed with both MC21 (using unmodified JENDL/AN-2005 evaluations for ^{17}O and ^{18}O) and SOURCES-4C, compared with experimental results from 1967 measurements by

Herold [24] and two separate experimental measurements by Anderson [25,26]. Data from all sources have been converted to specific neutron emission density [neutrons/(s·eV·g PuO_2)] in order to allow for a fair comparison between the different spectra. Experimental results from the measurements performed by Anderson were reported as relative neutron intensity rather than absolute neutron emission rate. For consistency, this data was renormalized to match the peak absolute neutron emission density value reported by Herold.

As noted previously, the PuO_2 composition used in the MC21 and SOURCES-4C simulations matches the specification reported by Herold [24]. The experiments by Anderson, however, both used PuO_2 samples that were isotopically enriched in ^{18}O . The 1967 experiment used enriched oxygen with 45.61% ^{18}O atom fraction, whereas the 1980 experiment used a sample with ^{18}O enrichment of 31% atom fraction. Although differences in ^{18}O enrichments affect the total (α, n) neutron production rates, the impact on the shapes of the neutron energy emission spectra after common normalization is negligible. Thus, a reasonable comparison of the neutron emission spectra from the three experiments can be made to the MC21 and SOURCES-4C results.

Inspection of Fig. 5 once again shows that the MC21 calculation using the Kalbach–Mann systematics for secondary neutron distributions for ^{17}O and ^{18}O (α, n) produces a neutron emission spectrum that deviates significantly from the experimental measurements as well as from the spectrum calculated with SOURCES-4C. This observation is consistent with the results for UO_2 , as described in the previous example. Interestingly, Fig. 5 also shows that the MC21 calculation using modified (α, n) data with two-body kinematics for neutron emission from ^{17}O and ^{18}O produces an emission spectrum with a pronounced peak below 1 MeV, which is not present in the spectrum calculated with SOURCES-4C (or in the experimental spectra). The difference between the spectra from the two codes below 1 MeV appears to be tied to the treatment of the

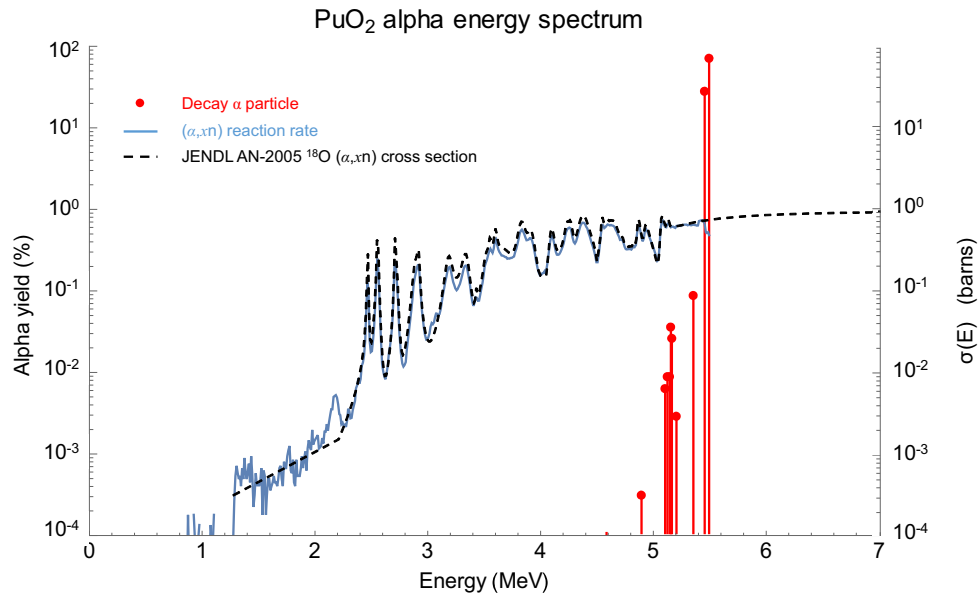


Fig. 4. Spectrum of alpha decay energies and (α, n) absorption rate for PuO_2 . Also shown is the microscopic total (α, n) cross section for ^{18}O , the dominant nuclide for (α, n) reactions, illustrating the relationship between the (α, n) reaction rate and cross section.

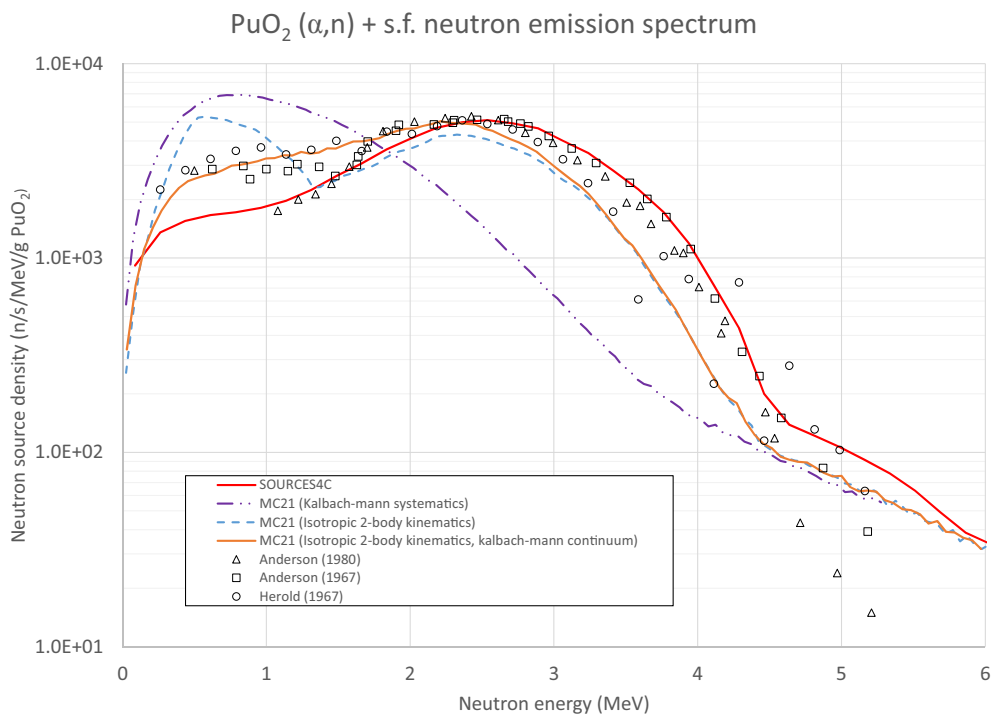


Fig. 5. Comparison of naturally occurring neutron emission spectrum, including (α, n) and spontaneous fission (s.f.), in PuO_2 between SOURCES-4C, MC21, and experimental results from Herold [24], Anderson [25], and Anderson [26].

energy state of the ^{21}Ne recoil following an $^{18}\text{O}(\alpha, n)$ reaction.

The JENDL/AN-2005 evaluation includes explicit cross section data for $^{18}\text{O}(\alpha, n)$ reactions that leave ^{21}Ne in the ground state or excited levels 1–4. A sixth “continuum” cross section is provided to account for $^{18}\text{O}(\alpha, n)$ reactions that leave the exiting ^{21}Ne nucleus above the fourth excited level (2.867 MeV). A plot of the JENDL/AN-2005 microscopic cross sections for the different $^{18}\text{O}(\alpha, n)$ reactions is shown in Fig. 6. Note that the JENDL evaluation suggests that the continuum reaction (e.g., reactions that leave ^{21}Ne above the fourth

excited level) becomes the most probable reaction for incident alpha energies above ~ 4.8 MeV, with a reaction branching fraction of $>30\%$ for alpha energies >5 MeV, and $>45\%$ for alpha energies above 6 MeV.

SOURCES-4C includes reaction branching fractions for $^{18}\text{O}(\alpha, n)$ reactions that leave ^{21}Ne in the ground state or excited levels 1–4, but does not include an additional continuum reaction that accounts for ^{21}Ne nuclei emitted above the fourth excited level. In addition, the reaction branching

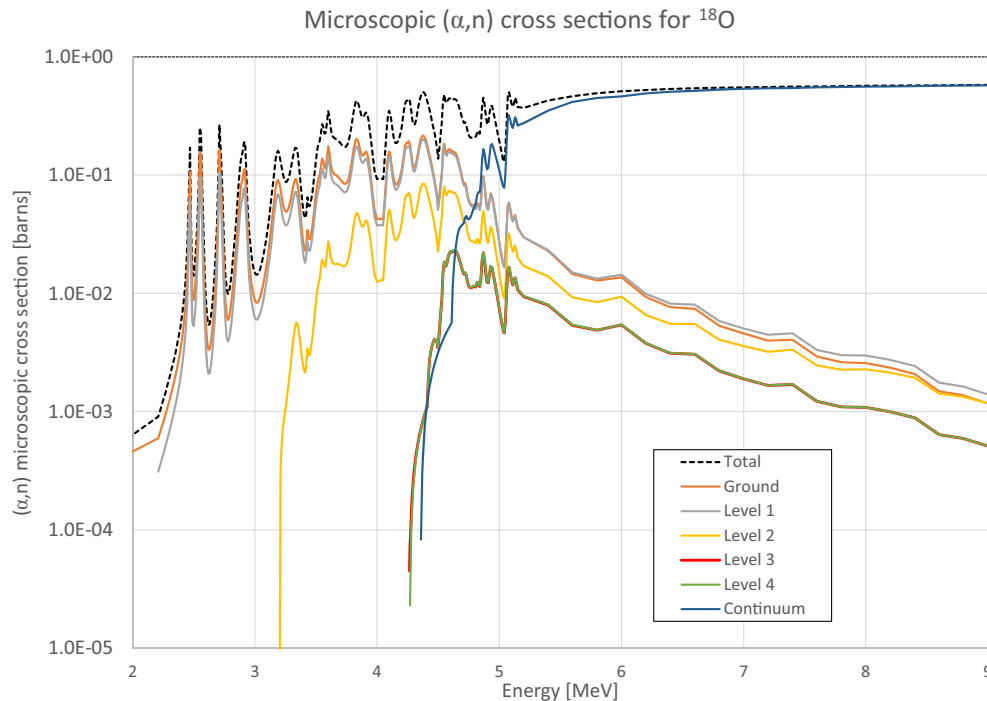


Fig. 6. JENDL/AN-2005 total and partial cross sections for ^{18}O (α,n) reactions.

fraction data in SOURCES-4C indicates that reactions involving the ground or first-excited state of ^{21}Ne remain dominant for all incident alpha energies. This data does not suggest the presence of a sharp change in the probability of leaving ^{21}Ne in a higher excited state for (α,n) reactions induced by alpha particles above 5 MeV.

The difference in the reaction branching fractions for incident alpha particles with energies above 5 MeV appears to lead to the different neutron emission spectra behavior predicted by MC21 and SOURCES-4C for neutron energies below 1 MeV. This conjecture would also explain why a corresponding spectral difference for low-energy neutrons is not observed in the UO_2 calculations, because the maximum decay alpha energy for uranium occurs just below 4.8 MeV.

Because Kalbach–Mann systematics were developed for high-energy incident charged particles, it may be expected that the neutron energy distribution defined for the continuum reaction (which has the highest threshold energy of the given partial level excitation reactions) may be more physical than the distributions given for the ground state and lower excitation level reactions. Furthermore, as the angular distribution of neutrons in the center-of-mass frame becomes more forward-peaked and anisotropic with increasing alpha energy, the isotropic two-body kinematics model may not perform adequately for continuum reactions with a high alpha-energy threshold. In order to test this hypothesis, special (α,n) libraries were produced for ^{17}O and ^{18}O where isotropic two-body kinematics are used to compute neutron energy distributions for the ground state and discrete level excitation reactions, but the original Kalbach–Mann systematics are used to compute the secondary neutron energy distributions for continuum reactions. The resulting spectrum, shown in Fig. 5, appears to be reasonably consistent with SOURCES-4C as well as with the experimentally observed spectra of Herold and Anderson. In any case, results from both the UO_2 and PuO_2 cases indicate that Kalbach–Mann systematics may not be physically appropriate to describe neutron energy distributions for (α,n) reactions induced by low-energy incident alphas typical of transuranic nuclide decay.

3.3. Manufactured Am–Be neutron source

For the final example, MC21 was used to calculate the neutron emission rate and spectrum from an Am–Be neutron source (the dominant commercially available type of artificial neutron source). The neutron source was modeled as a hollow stainless steel cylinder filled with a loose mixture of AmO_2 and Be powders. The cavity containing the active source material has a height of 4.826 cm and an inner diameter of 2.2225 cm. The composition of the homogenized source powder mixture is given in Table 3. All dimensions and composition information were taken from specifications for ~2.5 curie Am–Be neutron test sources manufactured by the Monsanto Research Corporation. The reference neutron source intensity for these sources was given as $4.5\text{--}6.0 \times 10^6$ neutrons/s.

The MC21 simulation for this case used 10,000 source alpha particles sampled from the alpha decay spectra of ^{241}Am , ^{242}Am , and ^{243}Am , again using the in-line decay source sampling capability in MC21. The birth weight of neutrons was set to 1×10^{-6} , which increases the number of sampled secondary (α,n) neutrons by a factor of 10^6 . The calculation used the JENDL/AN-2005 evaluation for alpha cross section data and the JEFF-3.1.1 evaluation for decay data. The JENDL/AN-2005 (α,n) reaction data for ^{17}O and ^{18}O were modified to use two-body kinematics with isotropic neutron emission in the center-of-mass frame, as described previously. Note

Table 3
Homogenized Am–Be composition definition.

Nuclide	Nuclide density [nuclides/(b·cm)]	Isotopic abundance (%)
^9Be	5.6311×10^{-2}	100.000
^{16}O	1.9825×10^{-4}	99.757
^{17}O	7.5517×10^{-8}	0.038
^{18}O	4.0739×10^{-7}	0.205
^{241}Am	9.3990×10^{-5}	94.613
^{242}Am	3.5725×10^{-6}	3.596
^{243}Am	1.7789×10^{-6}	1.791

that the JENDL (α, n) reaction for ^9Be was not modified, as the original evaluation used two-body kinematics with anisotropic angular data provided.

Results from the MC21 simulation estimate a decay source intensity of 9.623×10^6 alpha particles/s, with a corresponding (α, n) neutron source intensity of 5.138×10^6 neutrons/s, which is within the reference range given on the source specification. During the simulation, a total of 533,950 secondary neutrons were produced, with a cumulative weight of 0.5339. Fig. 7 shows the total (α, n) neutron emission spectrum in the Am–Be source, computed with both MC21 and SOURCES-4C. A comparison between the two emission spectra shows good agreement in the shape and locations of major peaks in the spectra, consistent with the level of agreement observed in the UO_2 and PuO_2 examples. The high energy tail of the neutron emission spectrum is attributable to the fact that the $^9\text{Be}(\alpha, n)$ reaction is exothermic with $Q = +5.701$ MeV when the recoil ^{12}C nucleus is left in the ground state.

Although Am–Be is traditionally modeled as a homogenized mixture of americium, oxygen, and beryllium atoms, some Am–Be source capsules are manufactured as a loose mixture of AmO_2 and Be powders. The size of the constituent particles that make up each powder affects alpha radiation transport within the material, impacting both the yield and energy distribution of neutrons emitted via (α, n) reactions. In Section 2.2, the concept of escape probability was introduced to account for alpha particles traveling through multiple materials before losing all of their energy (or dropping below the energy threshold for an (α, n) reaction). Here, the effect of material heterogeneity on alpha slowing-down and (α, n) reaction rate is assessed by modeling the Am–Be source as spherical AmO_2 particles embedded in a uniform background material of beryllium. Because no data regarding AmO_2 particle sizes were available, a sensitivity study was conducted using a range of AmO_2 particle diameters from 0.1 μm to 1,000 μm . In each case, the mass density of AmO_2 particles and beryllium was held constant at 11.680 g/cm^3 and 0.845 g/cm^3 , respectively. In addition, the volume fraction of AmO_2 was fixed at 0.388%, in order to maintain the original nuclide densities given in Table 3.

During each MC21 simulation, source alpha particles from the decay of americium were produced uniformly within an AmO_2 particle. The distance to the AmO_2 particle surface was then explicitly calculated based on the diameter of the AmO_2 particle along with the location and direction of the sampled alpha radiation. Alpha radiation that reached the surface of the AmO_2 particle prior to losing all of their energy was transferred to the beryllium background material, and the slowing-down process continued. Once in the beryllium, the distance to the next AmO_2 particle was randomly sampled from a nearest neighbor distribution (NND) for uniform mixtures of rigid, nonoverlapping spheres in a homogeneous background material. In this situation, the NND follows an exponential distribution

$$p(x) = \lambda e^{-\lambda x}, \quad (22)$$

where λ is a rate parameter given by

$$\lambda = \frac{3}{4R} \frac{V}{1-V}, \quad (23)$$

and R and V represent the AmO_2 particle radius and AmO_2 volume fraction, respectively [27]. The process of sampling distances traveled through the AmO_2 and beryllium materials was then repeated until the alpha energy was reduced below the energy threshold for all (α, n) reactions in ^9Be , ^{17}O , and ^{18}O .

Results for the (α, n) neutron production rate are shown in Table 4 for a homogeneous Am–Be material and five heterogeneous AmO_2/Be powder mixtures with AmO_2 particle diameters between 0.1 μm and 1,000 μm . These results demonstrate that the neutron source strength decreases as AmO_2 particle size is increased, effectively preventing some alpha particles from escaping the AmO_2 particle and reaching the beryllium material, which has a higher (α, n) cross section. The results also suggest that AmO_2 particle diameters ≤ 1 μm produce neutron source rates that are consistent with the reference range of $4.5\text{--}6.0 \times 10^6$ neutrons/s for this configuration. Although detailed manufacturing data regarding AmO_2 powder is not available, particle sizes of less than 1 μm are not unreasonable.

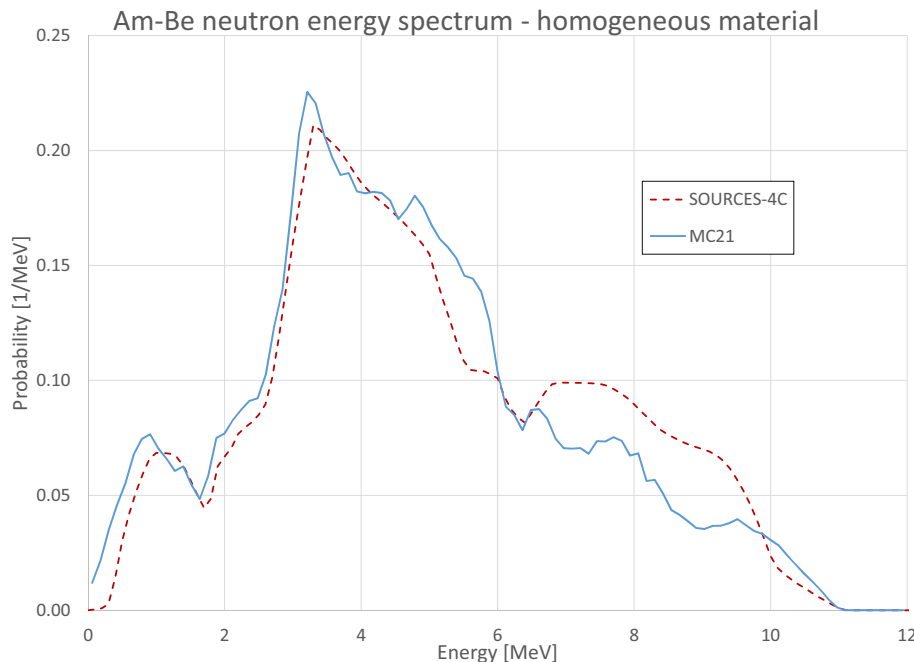


Fig. 7. Energy spectrum for neutrons produced via (α, n) reactions in a Am–Be source as calculated by the in-line (α, n) source sampling methodology implemented in MC21 (blue) and the SOURCES-4C computer code (red).

Table 4

Neutron emission rate for mixtures of AmO₂ and Be powders for various AmO₂ particle diameters.

AmO ₂ diameter (μm)	(α,n) Source (neutrons/sec)
Homogenized Am–Be	5.138×10^6
0.1	4.865×10^6
1.0	4.424×10^6
10.0	1.309×10^6
100.0	1.380×10^5
1,000.0	1.564×10^4

Fig. 8 shows the (α,n) neutron emission spectrum for the homogeneous Am–Be mixture, as well as the five heterogeneous mixtures each with different AmO₂ particle diameters. The results show that as the AmO₂ particle diameter increases, the neutron spectrum below 4 MeV shifts slightly toward lower energies, suggesting increased (α,n) reactions with ¹⁸O as a result of fewer alpha particles reaching the beryllium material. Note that, even for very large AmO₂ particle sizes, alpha particles born near the particle surface are able to reach the beryllium, producing the characteristic high energy tail in the neutron emission spectrum due to ⁹Be(α,n) reactions.

The results from this test provide a qualitative indication that the alpha escape model in the proposed method is working as intended and can capture the detailed effects of material heterogeneity on alpha transport. It is also worth noting that Am–Be sources also emit gamma rays due to the decay of ¹²C atoms that are left in an excited state following ⁹Be(α,n) reactions. Although gamma emission was not included as a part of this study, it should be possible to adapt the proposed in-line (α,n) sampling methodology to incorporate the subsequent decay of these excited recoil nuclei. Furthermore, (α,n) reactions that use two-body kinematics have enough data to model the characteristic gamma emission spectra associated with each excited level of the recoil nucleus as well as the effect of recoil nucleus motion on the gamma emission spectrum. Such an extension to the proposed model could allow accurate characterization of all radiations emitted from

manufactured sources, enabling improved modeling of experiments involving these types of sources.

4. Conclusions

A new in-line method for sampling neutrons emitted in (α,n) reactions based on alpha particle source information has been developed for continuous-energy MC simulations. The new method uses a continuous-slowing-down model coupled with cross section data to precompute expected neutron yields over the alpha particle lifetime. This eliminates the complexity and cost associated with explicit charged particle transport. When combined with an integrated alpha particle decay source sampling capability, the proposed algorithm provides an efficient and accurate method for sampling neutrons produced via (α,n) reactions based solely on nuclide inventories in the problem, with no additional user input required. Results from three example problems show that the proposed method adequately reproduces the (α,n) neutron yields and spectra from reference experiments and calculations.

All MC21 simulations in this work used the JENDL/AN-2005 nuclear data library, which provides evaluated cross section and energy-angle distribution data for (α,n) reactions for 17 isotopes. The majority of nuclide evaluations in JENDL/AN-2005 utilize Kalbach–Mann systematics to describe energy-angle spectra for neutron emission by (α,xn) reactions. For nuclides examined in this work, the neutron energy distributions predicted by Kalbach–Mann were biased much too low in energy when compared to experimental measurements. Consequently, a decision was made to use two-body kinematics, based on isotropic center-of-mass neutron emission, to determine energy spectra for neutrons produced via (α,xn) reactions. With this method, in certain cases, the partial cross section branching ratios in the evaluated nuclear data also resulted in overrepresentation of low-energy neutron emission (but to a lesser extent). In all cases, the energy spectra resulting from MC21 simulations based on two-body kinematics were superior to those based on Kalbach–Mann systematics in reproducing experimental measurements.

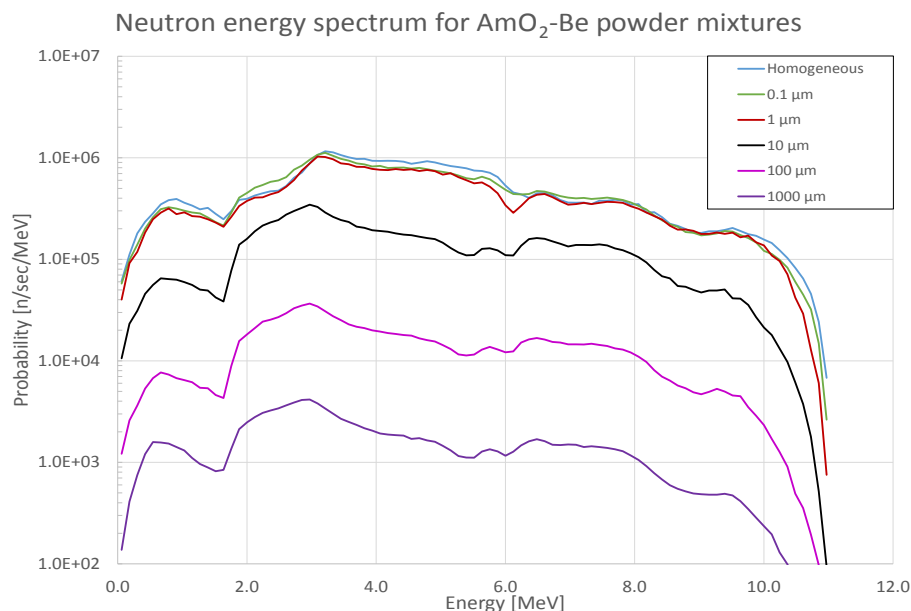


Fig. 8. Energy spectrum for neutrons produced via (α,n) reactions in a heterogeneous mixture of AmO₂ and Be powders, assuming various AmO₂ particle diameters. The neutron spectrum for a homogeneous Am–Be source is also shown for reference. These spectra are normalized by the alpha source intensity.

Although the proposed in-line method can allow efficient and accurate characterization of (α ,n) neutron emission in MC transport codes, the success of the approach is governed by the accuracy of supplied (α ,n) nuclear reaction data (as well as the supplied nuclear decay data used to compute α -particle emission). Revisiting the (α ,n) nuclear data evaluation process may improve the ability to predict neutron energy spectra from (α ,n) reactions induced by lower-energy alphas associated with transuranic nuclides, which is of interest in nuclear reactor and fuel cycle applications.

Conflicts of interest

The authors affirm that they do not have any potential conflicts of interest related to this research.

Acknowledgments

The authors acknowledge Mr. Dave Heinrichs and Dr. Ed Lent from Lawrence Livermore National Laboratory Nuclear Criticality Safety Division for their feedback, suggestions, and confirmatory calculations using the COG Monte Carlo code. The authors are especially indebted to Dave and Ed for their suggestion on using the Kalbach–Mann data, rather than two-body kinematics, for continuum reactions where level-specific data was not available.

References

- [1] D.B. Pelowitz (Ed.), MCNP6™ User's Manual, Version 1.0, LA-CP-1300634, Rev. 0, Los Alamos National Laboratory, Los Alamos, NM, 2013.
- [2] A. Ferrari, P. Sala, A. Fasso, J. Ranft, FLUKA: A Multi-Particle Transport Code, Version 2011, CERN-2005-010, CERN, Geneva, Switzerland, 2011.
- [3] M. Kutt, M. Englert, Increased transparency in simulations of measurements for nuclear disarmament verification, in: Proc. 35th ESARDA Symposium, Bruges, Belgium, 2013.
- [4] J.F. Ziegler, J.P. Biersack, M.D. Ziegler, SRIM — The Stopping and Range of Ions in Solids, ISBN 0-9654207-1-X, 2008, Pergamon, New York.
- [5] COG User's Manual, UCRL-TM-202590, Lawrence Livermore National Laboratory, Livermore, CA, 2002.
- [6] W.B. Wilson, R.T. Perry, E.F. Shores, W.S. Charlton, T.A. Parish, G.P. Estes, T.H. Brown, E.D. Arthur, M. Bozoian, T.R. England, D.G. Madland, J.E. Stewart, SOURCES 4C: A Code for Calculating (α ,n), Spontaneous Fission, and Delayed Neutron Sources and Spectra, LA-UR-02-1839, Los Alamos National Laboratory, Los Alamos, NM, 2002.
- [7] E.M. Lent, Alpha Transport in COG, LLNL-TR-655365, Lawrence Livermore National Laboratory, Livermore, CA, 2014.
- [8] F.S. Alsmiller, G.M. Estabrook, Neutron Yields from (α ,n) Reactions, ORNL-3016, Oak Ridge National Laboratory, Oak Ridge, TN, 1960.
- [9] H. Bethe, Passage of radiation through matter, in: I.E. Segre (Ed.), Experimental Nuclear Physics, John Wiley & Sons, New York, 1953, pp. 166–357.
- [10] V. Nitzki, H. Matzke, Stopping power of 1–9 MeV He⁺⁺ ions in UO₂, (U,Pu)O₂, and ThO₂, Phys. Rev. 8 (1973) 1894–1900.
- [11] J.L. Boles, R.S. Hafner, L.E. Fischer, Neutron Source Strength Estimates from (α ,n) Reactions in Binary Mixtures of Actinide Particles and Light Element Particles, UCRL-CONF-212717, Lawrence Livermore National Laboratory, Livermore, CA, 2005.
- [12] T. Murata, H. Matsunobu, K. Shibata, Evaluation of the (α ,xn) Reaction Data for JENDL/AN-2005, JAEA-Research 2006-052, Japan Atomic Energy Agency, 2006.
- [13] C. Kalbach, F.M. Mann, Phenomenology of continuum angular distributions: I. Systematics and Parametrization, Phys. Rev. C 23 (1981) 112–123.
- [14] C. Kalbach, Systematics of continuum angular distributions: extensions to higher energies, Phys. Rev. C 37 (1988) 2350–2370.
- [15] M. Herman, A. Trkov, D.A. Brown, ENDF-6 Formats Manual, ENDF-102/BNL-90365–92009, Rev. 2, 2011.
- [16] D.P. Griesheimer, D.F. Gill, B.R. Nease, T.M. Sutton, M.H. Stedry, P.S. Dobref, D.C. Carpenter, T.H. Trumbull, E. Caro, H. Joo, D.L. Millman, MC21 v.6.0 — a continuous-energy Monte Carlo particle transport code with integrated reactor feedback capabilities, Ann. Nucl. Energy 82 (2015) 29–40.
- [17] K.W. Geiger, L. van der Zwan, An Evaluation of the 9Be(α ,n) Cross Section, National Research Council Canada, 1976. NRCC-15303.
- [18] R.T. Perry, W.B. Wilson, Neutron Production from (α ,n) Reactions and Spontaneous Fission in ThO₂, UO₂, and (U,Pu)O₂ Fuels, LA-8869–MS, Los Alamos National Laboratory, Los Alamos, NM, 1981.
- [19] J.K. Bair, J. Gomez Del Campo, Neutron yields from alpha-particle bombardment, Nucl. Sci. Eng. 71 (1979) 18–28.
- [20] D. West, A.C. Sherwood, Measurements of thick-target (α ,n) yields from light elements, Ann. Nucl. Energy 9 (1982) 551–577.
- [21] D.P. Griesheimer, B.R. Nease, Improved weight window variance reduction for coupled radiation Monte Carlo transport calculations, in: Proc. PHYSOR 2016, Sun Valley, ID, May 1–5, 2016, American Nuclear Society, 2016 (CD-ROM).
- [22] D.P. Griesheimer, S.C. Marin, P.K. Romano, M.H. Stedry, Integrated decay source capability for large-scale Monte Carlo radiation transport calculations, in: Proc. PHYSOR 2016, Sun Valley, ID, May 1–5, 2016, American Nuclear Society, 2016 (CD-ROM).
- [23] G.J.H. Jacobs, H. Liskien, Energy spectra of neutrons produced by α -particles in thick targets of light elements, Ann. Nucl. Energy 10 (1983) 541–552.
- [24] T.R. Herold, Neutron spectrum of ²³⁸PuO₂, Nucl. Appl. 4 (1968) 19–22.
- [25] M.E. Anderson, Neutron Energy Spectra of ²³⁹Pu–Be, ²³⁸Pu–F, and ²³⁸Pu–¹⁸O(α ,n) Sources MLM-1422/TID-4500, Mound Laboratory, 1967.
- [26] M.E. Anderson, Neutron energy spectra of a ²³⁸Pu–¹⁸O(α ,n) source — unmoderated and polyethylene moderated, Health Phys. 39 (1980) 537–542.
- [27] B. Lu, S. Torquato, Chord-length distribution function for two-phase random media, Phys. Rev. E 47 (1993) 2950–2953.